Chemical Physics Letters 810 (2023) 140207

Contents lists available at ScienceDirect

Chemical Physics Letters

journal homepage: www.elsevier.com/locate/cplett

Unraveling the complexation effect of electron transporting materials with Liq on the charge transport properties: A theoretical perspective

Sunwoo Kang [a,*], Sang Ho Jeon [a], Taekyung Kim [b,c,*]

[a] Display Research Center, Samsung Display Co., 1 Giheung-gu, Gyunggi, South Korea
[b] Dept. of Information Display, Hongik University, Seoul 04066, South Korea
[c] Department of Materials Science and Engineering, Hongik University, Sejongsi 30016, South Korea

ARTICLE INFO

Keywords:
Density functional theory simulation
Charge transport property
ETL-Liq complex
Stabilization energy

ABSTRACT

The effect of coordinated structures of electron transporting materials (**ETM**s) with lithium quinolate (**Liq**) on charge transport characteristics was theoretically investigated. The reorganization energies of holes (λ_h) and electrons (λ_e) of **ETM-Liq** simultaneously increased compared with those of ETMs, indicating that the charge transporting is retarded. Interestingly, λ_e of **ETM-(Liq)**$_n$ increased, while λ_h decreased. Regarding transfer integrals for holes (t_h) and electrons (t_e), t_h's of **T2T-Liq** and **BPyTP2-Liq** were significantly reduced with t_e of **T2T-Liq** decreasing tremendously. Consequently, the hopping rates of holes of **Liq**-complexes were reduced, while that of electrons of **BPyTP2-Liq** increased and that of **T2T-Liq**/**TSPO1-Liq** was reduced.

1. Introduction

Ever since the gradual requirement for high-quality and evolutional form factors in the display and electronic device industries, organic light emitting-diodes (OLEDs) have received tremendous attention due to their fascinating advantages, including their flexibility, color purity, view angle, and contrast [1–4]. Accordingly, OLED devices have been becoming the most popular display technology in both mobile and TV display industries. To meet growing device efficiency and lifetime demands in the display industry, the OLED device architecture has been developed over time, evolving from simple-layered to multi-layered structures. Also, organic materials have been synthesized with the aim of improving the carrier transport and photophysical properties. Among the several representative examples, lithium quinolate (**Liq**), which is utilized in practice as an additive in electron transport layers (**ETL**s), has been primarily used to simultaneously fulfill high efficiency and prolong lifetime of OLED devices [5–7]. The specific effect of **Liq** on the efficiency and lifetime can be understood in that it helps inject electron carriers from the cathode and interrupts the transport of large amounts of electron carriers to emissive layers (EMLs). Accordingly, the charge carriers then become balanced, leading to the eventual lowering of the probabilities of exciton–exciton and exciton–polaron annihilations in the EMLs. It has been briefly understood that the electron mobility of **Liq** is so slow that it interrupts the generation of the fast pathway transport of electron carriers in the **ETL** matrix [8]. However, current understanding of the interruption of electron carrier transport into EMLs is insufficient in terms of the co-deposition of **Liq** in the **ETL** matrix. In terms of molecular structure, triazine functional groups, which are six-membered resonance structures consisting of three carbon (C) and nitrogen (N) atoms, have commonly been utilized as the backbone in the design and synthesis of **ETL** materials due to their excellent advantages of a strong electron acceptability and structural planarity [9,10]. Moreover, **ETL** materials with pyridine/pyrimidine/phosphine as their core structures have also been occasionally reported [11–15]. It is generally well-known that lone pair electron in nitrogen or oxygen atoms, acting as a Lewis base, can form a coordination bond with metal or Lewis-acid atoms. Therefore, it is expected that the complex structure of **Liq** and **ETL** materials can be sufficiently formed by mixing solid matrix. Furthermore, structural relaxation could be enhanced relative to the non-coordinated structure of **ETL**s upon the forming of such a coordination bond due to the increase in the degrees of freedom in the vibration and rotation movements. In a recently published paper, the complexation of **ETL** (BPhen) and **Liq** was proved by analyses of the Gibbs – DiMarzio prediction and X-ray photoelectron spectroscopy[16]. This experiment clearly supports the purpose of our theoretical investigation to understand the effect of **ETL-Liq** complexation on the charge transport property.

In this work, representative **ETL** materials specifically **T2T** (2,4,6-tris

* Corresponding authors.
E-mail addresses: swkang821221@gmail.com (S. Kang), taekyung.kim@hongik.ac.kr (T. Kim).

https://doi.org/10.1016/j.cplett.2022.140207
Received 9 August 2022; Received in revised form 11 November 2022; Accepted 15 November 2022
Available online 20 November 2022
0009-2614/© 2022 Elsevier B.V. All rights reserved.

(biphenyl-3-yl)-1,3,5-triazine), **BPyTP2** (2,7-Di(2,2′-bipyridin-5-yl)triphenylene), and **TPSO1** (Diphenyl-4-triphenylsilylphenyl-phosphine oxide) were chosen to analyze the effect of forming a **Liq-ETL** complex on the carrier transport properties (See Scheme 1). Density functional theory (DFT) calculations for both **ETL** and **ETL-Liq** complex structures were conducted to investigate variations in reorganization energies, transfer integrals, and carrier hopping rates. Overall, we believe this theoretical research will help extend current knowledge of the effect of **Liq** on OLED device performance.

2. Theory and computation

DFT calculations were carried out by employing a non-local density functional of the Becke three-parameter Lee-Yang-Parr exchange functional (B3LYP), with Pople's triple-zeta potential and a double polarization function (6-311G**) implemented in the suite of Gaussian 09 code [17]. All molecular structures in neutral, cation, and anion states were fully optimized without symmetry constraints (C1), and their thermodynamic stabilities were verified by frequency calculations. According to the Marcus formalism [18], the properties of hole or electron carrier transport are critically influenced by the reorganization energy (λ_h or λ_e) and transfer integral (t_h or t_e). In detail, the hopping rates of hole and electron carriers inversely depend on the λ_h or λ_e values, whereas those are proportionally depending on t_h or t_e. The λ_h or λ_e values can be generally derived from Nelsen's four-point method using the following equations [19]:

$$\lambda_h = \left(\lambda_{neutral}^{cation} - \lambda_{cation}\right) + \left(\lambda_{cation}^{neutral} - \lambda_{neutral}\right) \tag{1}$$

$$\lambda_e = \left(\lambda_{neutal}^{anion} - \lambda_{anion}\right) + \left(\lambda_{anion}^{neutral} - \lambda_{neutral}\right) \tag{2}$$

The transfer integrals of the hole and electron carriers in the present work were calculated via fully optimized dimer conformations. To simply mimic the nature of an amorphous film state, Grimme's dispersive correction was utilized to describe the non-covalent interaction of neighboring molecules. Moreover, the energy splitting from the intermolecular polarization effect was considered to gain transfer integral in dimer structures. t_h and t_e can be expressed as shown in the following equation [20]:

$$t^{eff} = \frac{t_{12} - \frac{1}{2}(e_1 + e_2)S_{12}}{1 - S_{12}^2} \tag{3}$$

where t_{12}, e_1, and e_2 are matrix elements of the Hamiltonian system. S_{12} is the spatial electron density overlap integral between the two highest occupied molecular orbitals (HOMOs) or two lowest unoccupied molecular orbitals (LUMOs). To obtain the t_h and t_e, the several dimer structures were preferentially prepared, thereof these were fully optimized at the same level of theory with Grimme's dispersion correction (GD3) [21]. At the most stable optimized structures of dimer, the single point calculations for t_h and t_e were conducted with B3LYP/TZVP level of theory, as implemented in a suite of ADF program [22].

The field-independent carrier hopping rates were derived based on the Marcus formalism as expressed in Eq. (4).

$$k_{ET} = \frac{4\pi^2 t^2}{h}\sqrt{\frac{1}{4\pi\lambda k_B T}}exp\left(-\frac{(\lambda + \Delta G)^2}{4\lambda k_B T}\right) \tag{5}$$

where t, λ, k_B, h, T, and ΔG are the transfer integral, reorganization energy, Boltzmann constant, Plank constant, temperature, and Gibbs free energy, respectively.

In addition, the Huang-Rhys factor can also be utilized to calculate λ_h or λ_e. More importantly, it is helpful in analyzing the critical vibration modes which belongs to the increase or decrease of the structural relaxation energies during redox reactions. Therefore, the analysis of Huang-Rhys factor for reorganization energy helps to rationally design the materials that are required to control the reorganization energies. It can be expressed by the following equation:

$$\text{Huang} - \text{Rhys factor} = \frac{1}{2}\omega_i K_i^2 \tag{5}$$

where K_i is the shift vector, and ω_i is the vibrational frequency of the i-th normal mode. K_i, which can be defined as a dimensionless displacement vector, indicates structural variations between the initial and final state of the i-th normal mode [23,24].

3. Results and discussion

3.1. Geometries and binding nature

In the beginning, it is essential to identify the most favorable **ETL-(Liq)**$_n$ structure for use as a reference structure. Therefore, in the present study, the stabilization energies of **T2T**, **BPyTP2**, and **TSPO1** were calculated as a function of the **Liq** molecule. As shown in Fig. 1, the most favorable structures of **T2T** and **TSPO1** as **ETL-(Liq)**$_n$ could be determined **ETL-Liq** structure. However, the **ETL-(Liq)**$_2$ structure is the favorable conformation via the complexation of **BPyTP2** and **Liq**. To investigate the effect of **Liq** on the charge transport property of **ETL** materials, the **ETL-Liq** structure was chosen as the reference. The optimized structures of **ETL-Liq** complexes and their structural parameters are denoted in Fig. 2. Upon the formation of a coordination bond between the **ETL** and **Liq**, the structural planarity of **BPyTP2** (at a bipyridine moiety) and **T2T** (at a triazine moiety) was significantly altered, as coordinated **Liq** interrupts to form intramolecular H-bonds via repulsive interactions. On the other hand, important structural variations in the **TSPO-Liq** complex were not detected. The distances of the coordination bonds in the **T2T-Liq** (N-Li), **BPyTP2-Liq** (N-Li), and **TSPO1-Liq** (O-Li) complexes were calculated as 2.084, 2.054, and 1.850 Å, respectively. In contrast with **T2T** and **BPyTP2**, it was interesting to observe in the optimized structure that **Liq** seemed to form this coordinated structure based on a coordination bond (Li-O) and intermolecular H-bond (O…H).

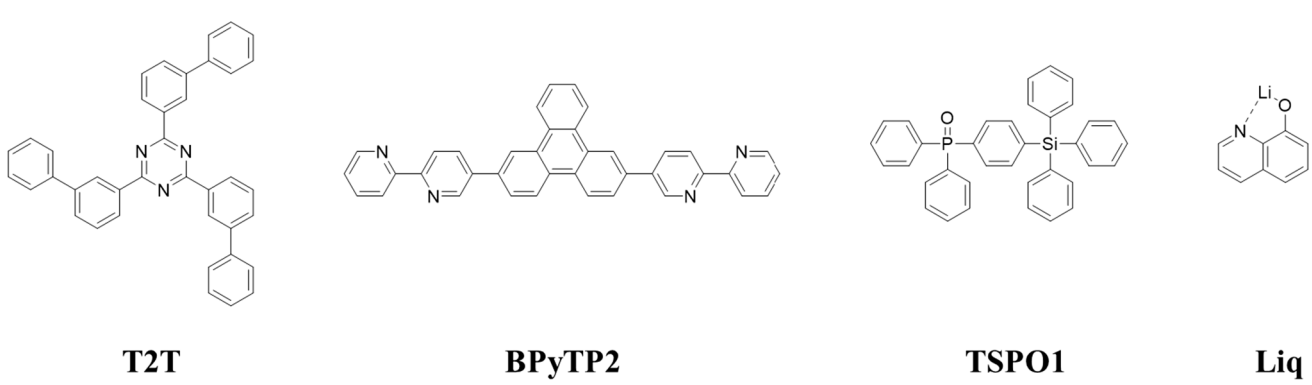

Scheme 1. 2D chemical structures of **ETL** and **Liq** materials 14.

SDC EX. 1030 - 2/8

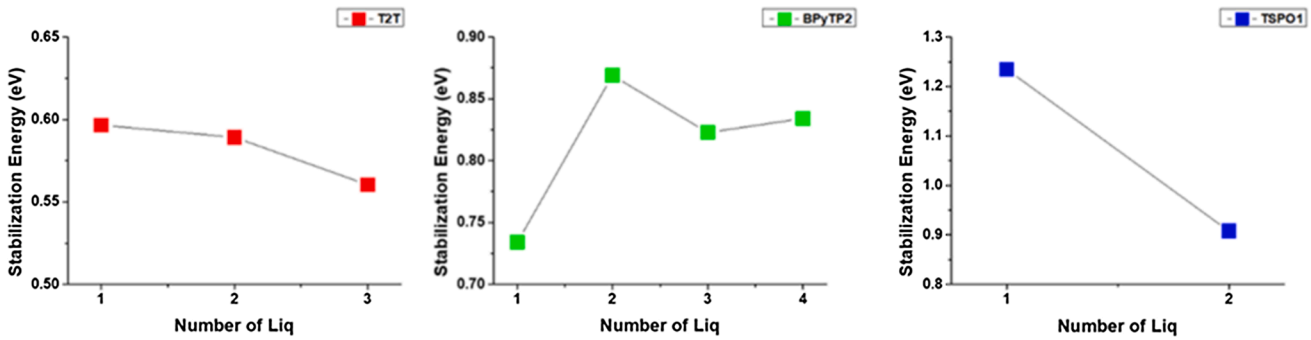

Fig. 1. Stabilization energies of **ETL-Liq** complexes as a function of the **Liq** molecule.

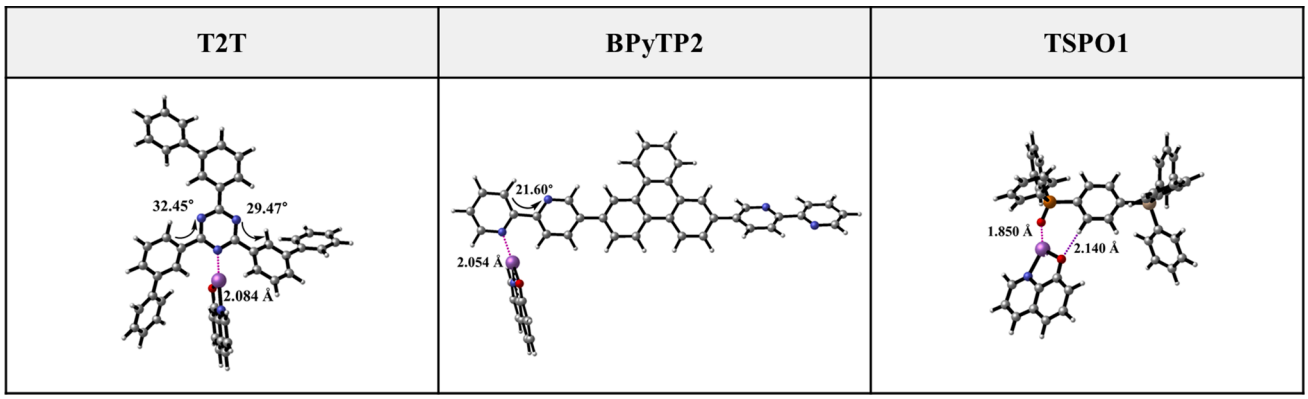

Fig. 2. Optimized structures of **ETL-Liq** complexes and their representative parameters.

The calculated values for the distance and angle of O…H-C in the **TSPO1-Liq** complex were found to be 2.140 Å and 158.54°, which represent the essential parameters of normal H-bonds, as shown in previous reports [25,26]. To clarify the existence of intermolecular H-bond in the **TSPO1-Liq** complex, a relaxed potential energy surface simulation (PES) was performed along the elongation of the O…H distance between the **Liq** and **TSPO1**. As shown in Fig. 3, the results indicate that the calculated energies of the optimized structures with respect to increases in the distance of O…H-C are gradually destabilized, indicating that the optimized structure of the **TSPO1-Liq** complex is the lowest energy point. The energy gap between the initial (with O…H-C) and final (without O…H-C) states was calculated as 0.130 eV (3.007 kcal/mol), which specifically indicates an attractive interaction via the O…H-C conformation in **TSPO1-Liq**. Overall, based on the results of the structural parameters and interaction energy, it was clarified that the O…H-C conformation in **TSPO1-Liq** can be characterized as a normal intermolecular H-bond. The binding energies of **T2T**, **BPyTP2**, and **TSPO1** with **Liq** were calculated as 0.597, 0.734, and 1.241 eV, respectively, corresponding to higher binding energy in order: **T2T** < **BPyTP2** < **TSPO1**. The behavior of the binding energies in these complexes could be understood based on the fact that the distances of N/O…Li bonds dominantly affect the strength of the binding energies.

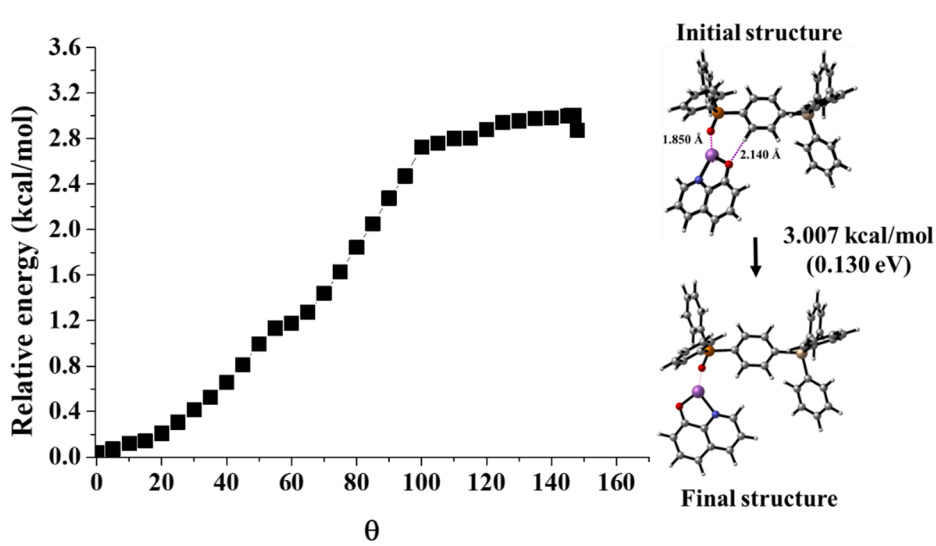

Fig 3. Results of potential energy surface simulation for **TSPO1-Liq**.

SDC EX. 1030 - 3/8

Furthermore, it was also found that the intermolecular H-bonds in **TSPO1-Liq** weakly assists in forming the strong binding energy between **TSPO1** and **Liq**.

The electronic structures of the **T2T**, **BPyTP2**, **TSPO1**, and their **Liq** coordinated complexes (**T2T-Liq**, **BPyTP2-Liq**, and **TSPO1-Liq)** are shown in Fig. 4. The **T2T** and **BPyTP2** materials without coordination of **Liq** showed excellent overlap of the highest occupied and lowest unoccupied molecular orbitals, which is known as the π-π transition property. However, TPSO1 exhibited the separated spatial distributions for the HOMO and LUMO, indicating the intramolecular charge transfer (CT) transition property. Moreover, the shapes of molecular orbitals inform the hopping sites of charge carriers in **ETL**s. Interestingly, the unique characteristics of these electronic structures changed when **Liq** was coordinated with the **ETL** materials. Specifically, in the electronic structures of **T2T-Liq**, **BPyTP2-Liq**, and **TSPO1-Liq**, it was illustrated that the spatial distribution of HOMO predominantly lies on the **Liq**, while the LUMO was mainly delocalized on the **ETL**. These spatial distributions can be attributed to the intermolecular CT transition. Also, the changes of electronic structures implies that the hopping site of charge carriers turned to be significantly variated in the **ETL-Liq** complexes.

3.2. Reorganization energies

As introduced in theory and computation, the λ_h and λ_e values for the **ETL** and **ETL-Liq** materials were calculated using Nelsen's four-point method. All the calculated λ_h and λ_e values are listed in Table 1. The λ_h values for **T2T**, **BPyTP2**, and **TSPO1** were calculated as 0.136, 0.229, and 0.454 eV, respectively. In addition, the calculated λ_e values for **T2T**, **BPyTP2**, and **TSPO1** were 0.275, 0.302, and 0.499 eV, respectively. Interestingly, upon the reversible redox reaction ($\lambda_h = M \rightarrow M^+/M^+ \rightarrow M$ and $\lambda_e = M \rightarrow M^-/M^- \rightarrow M$), it was found that each energy relaxation process under oxidative and reductive reactions differently contributed to the λ_h and λ_e values. For λ_h, the structural relaxation energies of **T2T** and **BPyTP2** under $M \rightarrow M^+/M^+ \rightarrow M$ reactions were equally calculated, whereas, in the case of TPSO1, the energy contribution of the $M^+ \rightarrow M$ reaction (0.163 eV) was found to be relative to the $M \rightarrow M^+$ reaction (0.291 eV). Otherwise, the calculated λ_e was equally attributed to each relaxation energy during $M \rightarrow M^-/M^- \rightarrow M$ reactions. Understanding

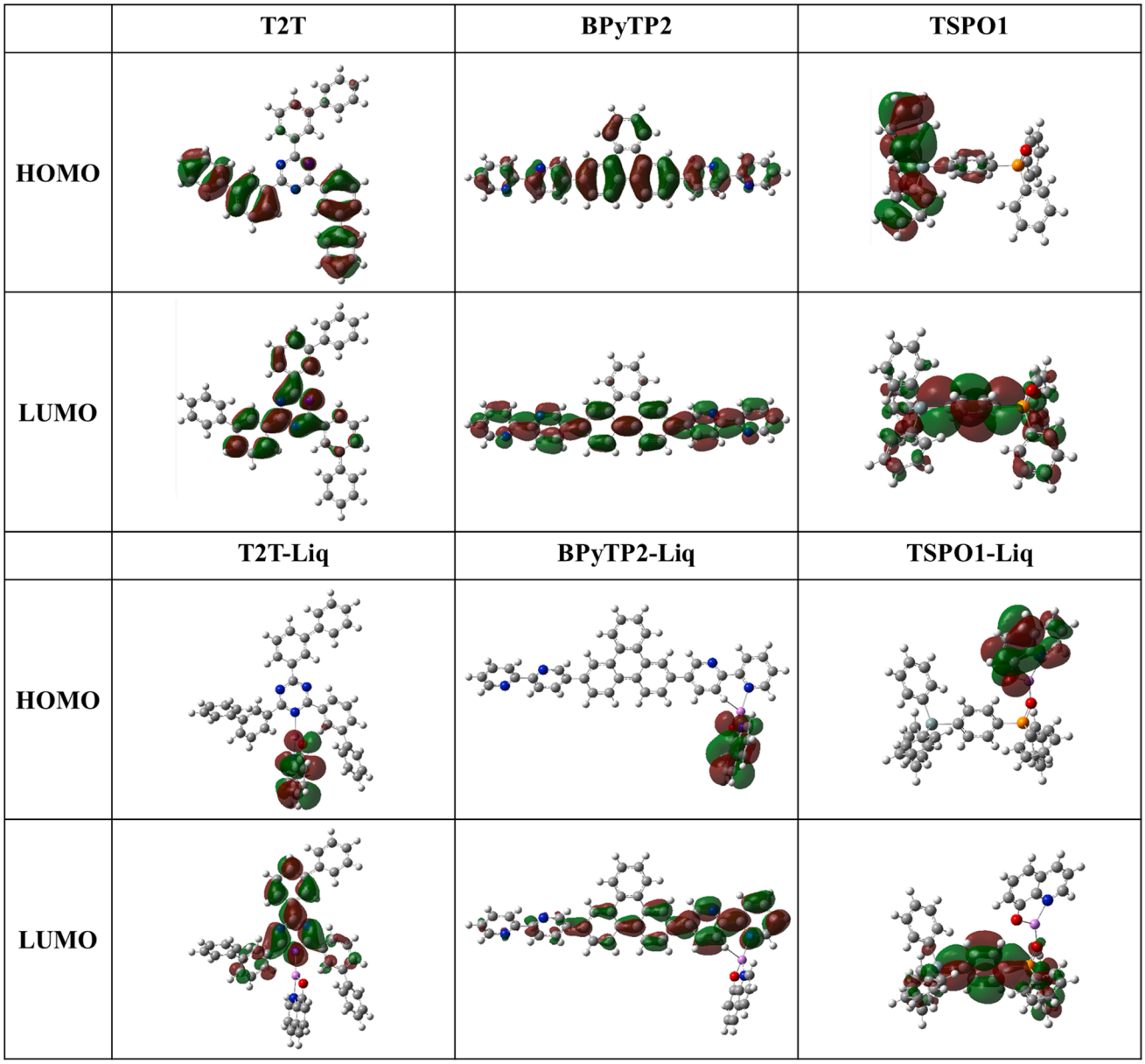

Fig. 4. Spatial distribution of HOMO and LUMO in **ETLs** and **ETL-Liq** complexes.

SDC EX. 1030 - 4/8

Table 1
Charge transport properties of the **ETL** materials and **ETL-Liq** complexes.

ETL						
	λ_h	λ_e	t_h^2	t_e^2	k_h	k_e
T2T	**0.136**	**0.275**	**5.50*10^{-4}**	**3.38*10^{-3}**	**6.69*10^{12}**	**7.47*10^{12}**
BPyTP2	**0.229**	**0.302**	**5.54*10^{-5}**	**2.15*10^{-5}**	**2.10*10^{11}**	**3.50*10^{10}**
TSPO1	**0.454**	**0.499**	**1.35*10^{-6}**	**1.59*10^{-5}**	**4.07*10^{8}**	**2.94*10^{9}**
ETL-Liq						
	λ_h	λ_e	t_h^2	t_e^2	k_h	k_e
T2T	**0.515**	**0.395**	**3.36*10^{-7}**	**1.23*10^{-6}**	**5.24*10^{7}**	**7.06*10^{8}**
BPyTP2	**0.283**	**0.365**	**1.46*10^{-6}**	**4.26*10^{-4}**	**2.93*10^{9}**	**3.42*10^{11}**
TSPO1	**0.573**	**0.952**	**1.39*10^{-4}**	**1.61*10^{-4}**	**1.17*10^{8}**	**2.62*10^{8}**

the origin of λ_h and λ_e, which corresponds to the vibration coupled structural relaxation energy via the redox reaction, can be achieved using the Huang-Rhys factor. The advantage of the analysis of Huang-Rhys factor has been known that it is one of useful methodology to understand the contribution of specific vibration mode on the reorganization energy. Accordingly, the origin of the different relaxation energies of **TSPO1** on λ_h was further investigated using the Huang-Rhys factor. As can be seen in Fig. 5, the vibration mode at 23.05 cm^{-1}, which can be attributed to the C—H not being in the plane bending mode, is drastically activated during the M → M$^+$ reaction. Based on these findings, it can be speculated that the intermolecular H-bonds of **T2T** and **BPyTP2** may play an essential role in determining the balanced structural relaxation energies. In addition to this, we further characterized key vibration modes strongly related to the determination of the λ_h and λ_e values of **T2T**, **BPyTP2**, and **TSPO1**. Specifically, in **T2T**, C—H out-of-plane, in-plane bending, and C—C stretching vibration modes took on important roles in determining λ_h. For λ_e, the C-N stretching vibration mode was predominantly activated under the M → M$^-$ reaction, whereas the deactivation of C—N stretching vibration modes and the activation of C—H in-plane and C—C stretching vibration modes occurred under the M$^-$ → M reaction. For the λ_h and λ_e of **BPyTP2**, C—H out-of-plane bending and C—C stretching vibration modes mainly contributed to the relaxation energy process via hole and electron carrier transport. In the case of the λ_h and λ_e of **TSPO1**, C—H out-of-plane bending vibration modes solely contributed to the λ_e.

We will now discuss the results regarding the λ_h and λ_e values in the **ETL-Liq** complexes. The λ_h of **T2T-Liq** was calculated to be 0.573 eV, which is ~ 3.8 times larger than that of **T2T**. On the other hand, the calculated λ_h values of **BPyTP2-Liq** and **TSPO1-Liq** were 0.283 and 0.573 eV, which were slightly increased up to 124 % and 126 % relative to **BPyTP2** and TPSO1. Accordingly, it was expected that the hopping rate of the hole carrier in the **ETL** matrix might be negatively affected by the complexation of **ETL** and **Liq** materials. This result also indicated that forming a **ETL-Liq** complex helps to reduce the probability of hole leakage from the EMLs. Similar to the behaviors of λ_h, the calculated λ_e values of **T2T-Liq**, **BPyTP2-Liq**, and **TSPO1-Liq** were entirely increased compared to those of structures without **Liq**. Specifically, the λ_e of **T2T-Liq** and **BPyTP2-Liq** were calculated as 0.395 and 0.365 eV; these were increased up to 144 % and 121 % compared to **T2T** and **BPyTP2**. Particularly, the λ_e of **TSPO1-Liq** (0.952 eV) was approximately two-fold larger than that of **TSPO1**. Based on the comprehensive analyses of the λ_h and λ_e values of the **ETL** and **ETL-Liq** materials, it can be concluded that the complexation of **ETL** and **Liq** may simultaneously weaken the characteristics of the hole and electron carrier transport in the **ETL** matrix since the λ_h and λ_e values are inversely proportional to the hopping rates. Now, we will discuss the λ_h and λ_e findings for the **ETL-Liq** complexes. Specifically, the calculated λ_h of the **ETL-Liq** complexes were equally attributed to each relaxation energy during the M → M$^+$/M$^+$ → M reactions. Moreover, the calculated λ_e of **T2T-Liq** and **TSPO1-Liq** revealed the equal contribution of each relaxation energy during the M → M$^-$/M$^-$ → M reactions. However, in the case of **BPyTP2-Liq**, the relaxation energy during the M$^-$ → M reaction predominantly contributed to the determination of λ_e. To understand the nature of this disparate contribution of the relaxation energies during the M → M$^-$/M$^-$ → M reactions, the optimized structures of **BPyTP2-Liq** in both neutral and anion states were compared. In Fig. 4, it can be seen that **Liq** was

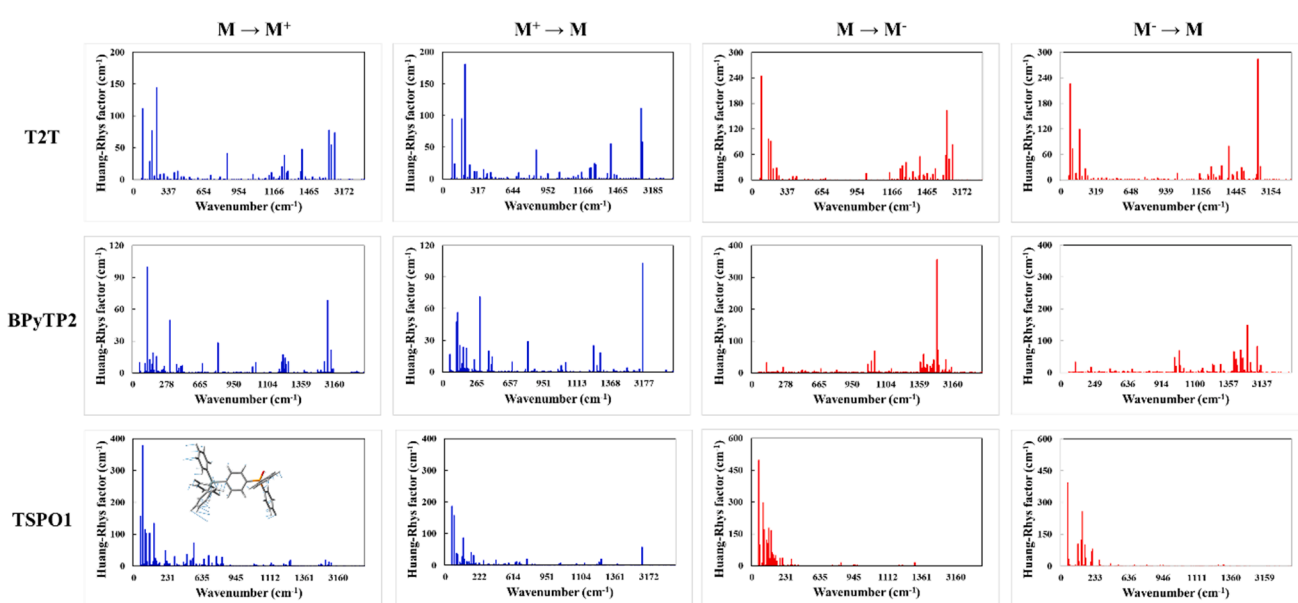

Fig. 5. Computed Huang-Rhys factor of the **ETL** materials via redox reaction.

SDC EX. 1030 - 5/8

perpendicularly coordinated to the pyridine moiety in the neutral state. However, as shown in Fig. 6, the coordinated structure was transformed toward horizontal conformation in the anion state. The reason may be related to the optimized structures in the anion state, which the Li-H coupling and intermolecular H-bond (O…H-C) probably supported in changing from perpendicular to horizontal conformations. To clearly identify the existence of intermolecular H-bond and Li-H coupling in the **BPyTP2-Liq** complex, PES calculations along the dihedral angle of O-Li…N-C and natural transition orbital (NTO) simulations were performed. As shown in Fig. 6, the calculated energies were gradually destabilized in accordance with the increase in the dihedral angle. The calculated energy gap between the minimum (with H-bond) and maximum (without H-bond) energies was 0.047 eV (1.085 kcal/mol). In addition, the calculated energy of the Li-H coupling was 0.164 eV based on the NBO calculation [27]. Based on these comprehensive analyses, the origin of the unequal processes of relaxation energy can be understood based on the energy of vertical electron absorption in a neutral structure being less favorable than that of vertical electron desorption depending on the existence of Li-H coupling and intermolecular H-bonds.

To clarify the interrelationship between the number of **Liq** molecules and the λ_h and λ_e values, the **ETL-(Liq)**$_n$ complexes were further analyzed. The results regarding the λ_h and $\lambda\lambda_e$ values are plotted in Fig. 7. In the case of the **T2T-(Liq)**$_n$ (n = 1–3) and **BPyTP2-(Liq)**$_n$ (n = 1–4) complexes, with an increase in the coordinated **Liq** molecules, the λ_h values tended to decrease while the λ_e values proportionally increased. Specifically, it can be noted that the λ_h values of **BPyTP2-(Liq)**$_n$ (n ≥ 3 and 4) and **T2T-(Liq)**$_n$ (n ≥ 2 and 3) were lower than those of **BPyTP2** and **T2T**. Furthermore, it can be expected that the hopping rate of the hole carrier can be advantageous as the number of **Liq** molecule increases. In contrast, the hopping rate of the electron carrier is disadvantageously affected by forming multiple coordination bonds with **Liq**. For **TSPO1-(Liq)**$_n$ (n = 1–2), the λ_h and λ_e values were reduced depending on the increase in the number of coordinated **Liq** molecules. Moreover, the calculated λ_h and λ_e values of the **TSPO1-Liq** complexes were still larger than those of the **ETL** materials although the calculated λ_h and λ_e values of **TSPO1-(Liq)**$_n$ (n = 1–2) were effectively reduced as a function of the **Liq** molecule. Overall, these results indicate that the electron carrier might be slowly transferred to neighboring molecules in a **Liq**-doped **ETL** matrix.

3.3. Transfer integral and hopping rate

According to the Marcus formalism, an effective orbital overlap between neighboring molecules is essentially required to obtain the hopping rate of charge carriers. Several types of dimer structures of **BPyTP2-Liq**, **T2T-Liq**, and **TSPO1-Liq** were calculated to obtain their stable optimized structures. As introduced in theory and computation, the transfer integral values (t_h^2 and t_e^2) were derived and are summarized in Table 1. As can be seen Fig. 8, the non-covalent interaction for the paired structures of **BPyTP2**, **T2T**, **BPyTP2-Liq**, and **T2T-Liq** can be mainly attributed to the π-π interactions, belonging to the part of ETMs moiety. However, for **TSPO1** and **TSPO1-Liq**, the π-π and π-H interactions were simultaneously affected to sustain the pair structures. Similar to the results for λ_h and λ_e, the t_h^2 and t_e^2 values of **T2T** and **BPyTP2** were considerably reduced after complexation with **Liq**. On the other hand, the t_h^2 and t_e^2 values of TPSO1-**Liq** were surprisingly enhanced relative to **TSPO1**. These differences can be understood based on the optimized structures of the intermolecular distances of **T2T-Liq** and **BPyTP2-Liq** being slightly elongated relative to those of **T2T** and **BPyTP2** in the dimer structures, resulting in the poor overlap of the molecular orbitals. However, in the case of **TSPO1** and **TSPO1-Liq**, the coordinated **Liq** enabled the close interaction with each monomer, improving the overlap of the spatial distribution of the molecular orbitals. Based on the calculated λ and t values, the hopping rates of the hole and electron carriers (k_h and k_e) were also derived using the Marcus formulation. The calculated k_h values of **T2T-Liq** and **BPyTP2-Liq** were smaller than those of **T2T** and **BPyTP2**, indicating slow hole carrier mobility. However, the k_h of **TSPO1-Liq** was higher relative to that of TPSO1. In terms of the electron carrier, the calculated k_e values of **T2T-Liq** and **TSPO1-Liq** were reduced relative to **T2T** and **TSPO1**. On the other hand, the k_e of **BPyTP2-Liq** was faster than that of **BPyTP2**. In the present work, it was indicated that the electron carrier mobilities of **T2T** and **TSPO1** were negatively affected by the co-deposition of **Liq**, in which **BPyTP2** may have enhanced electron carrier mobility.

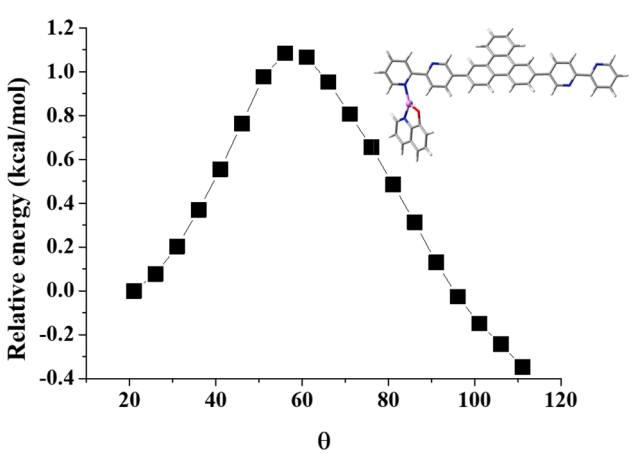

Fig. 6. Results of potential energy surface simulation of **BPyTP2-Liq** in the anion state.

4. Conclusion

In this study, the effect of **Liq** on the characteristics of hole/electron carrier transport via **Liq** deposition on the **ETL** matrix was theoretically investigated. It was found that a **ETL-Liq** complex could be formed from an attractive interaction between **ETL** and **Liq** through a coordination bond. In addition, stabilization energy calculations showed that **ETL-Liq** for **T2T/TSPO1** and (**ETL-Liq**)$_2$ for **BPyTP2** were the favorable complex structures. In terms of the λ_h and λ_e values of **ETL-Liq** and **ETL**s, forming a **ETL-Liq** structure leads to increases in both values, resulting in a negative effect on the hole/electron carrier transport. Moreover, as a function of the **Liq** molecule, the calculated λ_e of **T2T-(Liq)**$_n$ and **BPyTP2-(Liq)**$_n$ was continuously increased, while that of TPSO1-(**Liq**)$_n$ tended to decrease. However, the calculated λ_h values were equally diminished as a function of the **Liq** molecule. In terms of the transfer integral, the t_h and t_e values of **T2T-Liq** were decreased, while those of TPSO1-**Liq** were unexpectedly increased relative to their non-**Liq** coordinated structures. Moreover, in the case of **BPyTP2-Liq**, it was shown that t_h was calculated to be disadvantageous, but t_e was advantageously calculated. Eventually, the k_h values of all the **ETL-Liq** complexes were calculated to show a slowing trend. On the other hand, the k_e values of **T2T-Liq** and **TSPO1-Liq** (but not **BPyTP2-Liq**) were calculated as showing a decreasing trend. Based on the comprehensive consideration of these results, it can be concluded that the co-deposition of **Liq** in an **ETL** solid matrix generally weakens the characteristics of hole/electron carrier transport via forming an **ETL-Liq** complex.

5. Compliance with ethical standards.

The authors declare that they have no conflict of interest.

Declaration of Competing Interest

The authors declare that they have no known competing financial interests or personal relationships that could have appeared to influence the work reported in this paper.

SDC EX. 1030 - 6/8

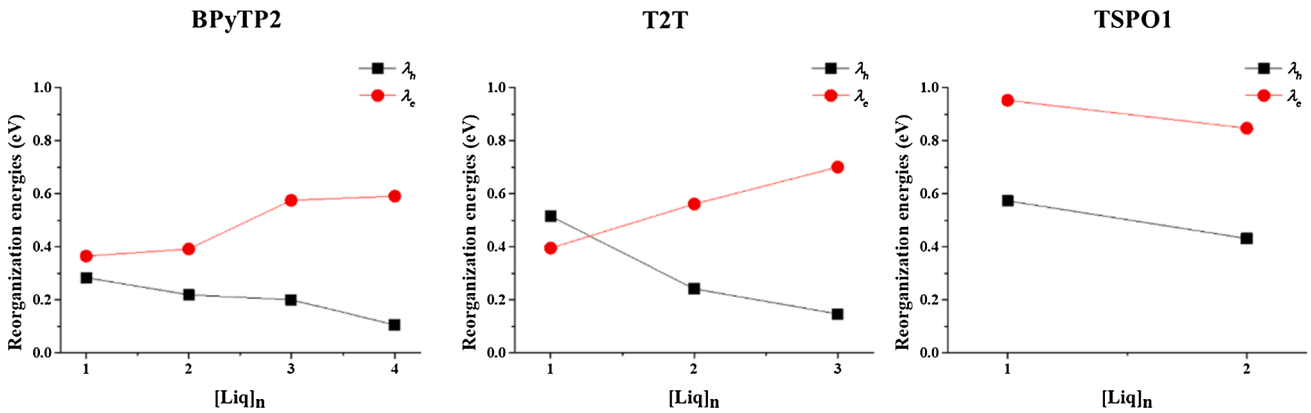

Fig. 7. Variations in reorganization energies of the hole and electron as a function of the **Liq** molecule.

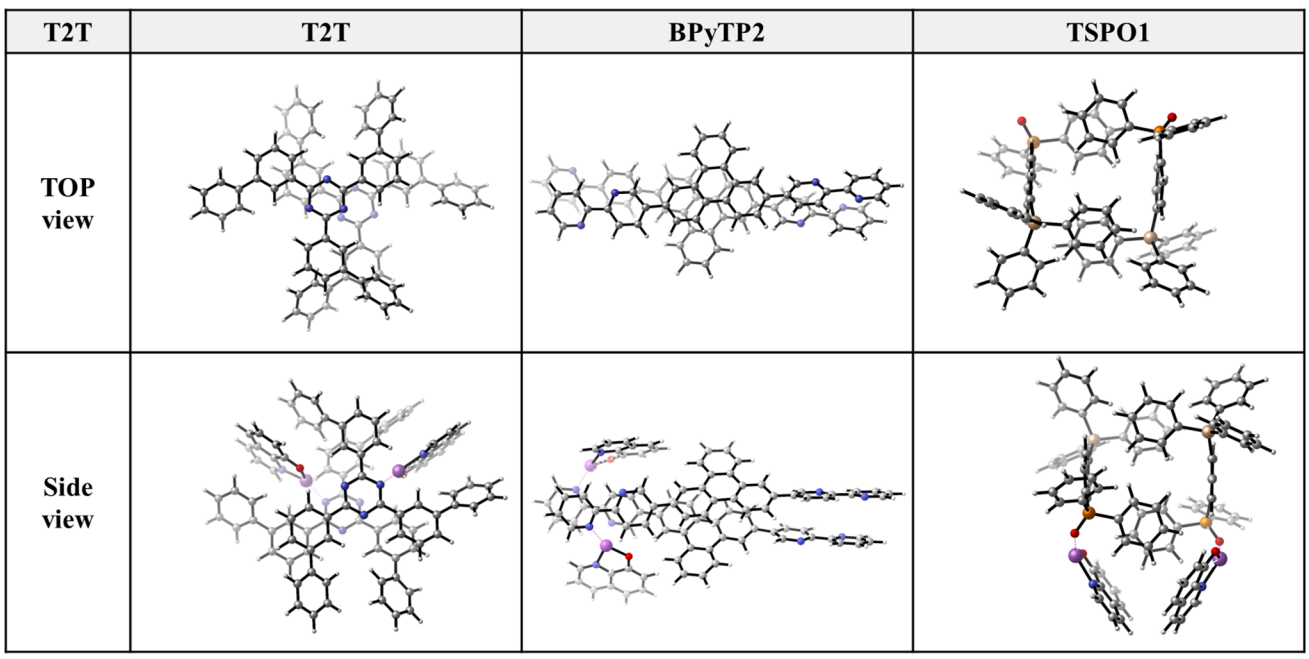

Fig. 8. Optimized dimeric structures of **T2T-Liq**, **BPyTP2-Liq**, and **TSPO1-Liq**..

Data availability

Data will be made available on request.

Acknowledgements

This work was supported by MOTIE (K_G012001605202 and K_G012002238601), the National Research Foundation of Korea (NRF) funded by Korean Government (No. 2022R1F1A1074304), and Samsung Display Co Ltd.

References

[1] H.-W. Chen, J.-H. Lee, B.-Y. Lin, S. Chen, S.-T. Wu, Light: Sci. Appl. 7 (2018) 17168.
[2] C.H. Chien, C.K. Chen, F.M. Hsu, C.F. Shu, P.T. Chou, C.H. Lai, Adv. Funct. Mater. 19 (2009) 560.
[3] X. Xing, L. Zhang, R. Liu, S. Li, B. Qu, Z. Chen, W. Sun, L. Xiao, Q. Gong, ACS Appl. Mater. Interfaces 4 (2012) 2877.
[4] K.J. Kim, K.M. Hwang, H. Lee, S. Kang, S.-B. Ko, M.-S. Eum, Y.K. Kim, T. Kim, J. Mater. Chem. C 9 (2021) 4029.
[5] C. Schmitz, H.-W. Schmidt, M. Thelakkat, Chem. Mater. 12 (2000) 3012.
[6] T. Chiba, Y.-J. Pu, T. Ide, S. Ohisa, H. Fukuda, T. Hikichi, D. Takashima, T. Takahashi, S. Kawata, J. Kido, ACS Appl. Mater. Interfaces 9 (2017) 18113.
[7] H.M. Kim, J.H. Seo, W.K. Han, K.H. Lee, H.J. Kang, S.S. Yoon, Y.K. Kim, Mol. Cryst. Liq. Cryst. 538 (2011) 53.
[8] A. Kumar, R. Srivastava, P. Tyagi, D. Mehta, M. Kamalasanan, J. Appl. Phys. 109 (2011), 114511.
[9] H.-F. Chen, T.-C. Wang, S.-W. Lin, W.-Y. Hung, H.-C. Dai, H.-C. Chiu, K.-T. Wong, M.-H. Ho, T.-Y. Cho, C.-W. Chen, J. Mater. Chem. 22 (2012) 15620.
[10] R.A. Klenkler, H. Aziz, A. Tran, Z.D. Popovic, G. Xu, Org. Electron. 9 (2008) 285.
[11] H.-W. Lin, C.-W. Lu, L.-Y. Lin, Y.-H. Chen, W.-C. Lin, K.-T. Wong, F. Lin, J. Mater. Chem. A 1 (2013) 1770.
[12] S.J. Su, Y. Takahashi, T. Chiba, T. Takeda, J. Kido, Adv. Funct. Mater. 19 (2009) 1260.
[13] S. Jang, S.H. Han, J.Y. Lee, Y. Lee, Synth. Met. 239 (2018) 43.
[14] B. Wang, X. Lv, B. Pan, J. Tan, J. Jin, L. Wang, J. Mater. Chem. C 3 (2015) 11192.
[15] A.L. Von Ruden, L. Cosimbescu, E. Polikarpov, P.K. Koech, J.S. Swensen, L. Wang, J.T. Darsell, A.B. Padmaperuma, Chem. Mater. 22 (2010) 5678.
[16] M.S. Ki, M. Sim, O. Kwon, K. Im, B. Choi, B.J. Cha, Y.D. Kim, T.Y. Jin, K. Paeng, ACS Materials Letters 4 (2022) 1676.
[17] M. Frisch, G. Trucks, H. Schlegel, G. Scuseria, M. Robb, J. Cheeseman, G. Scalmani, V. Barone, B. Mennucci, G. Petersson, Google Scholar There is no corresponding record for this reference (2015).
[18] R.A. Marcus, Rev. Mod. Phys. 65 (1993) 599.
[19] S.F. Nelsen, S.C. Blackstock, Y. Kim, J. Am. Chem. Soc. 109 (1987) 677.
[20] S. Kang, J.H. Moon, T. Kim, J.Y. Lee, RSC Adv. 9 (2019) 27807.
[21] S. Ehrlich, J. Moellmann, W. Reckien, T. Bredow, S. Grimme, ChemPhysChem 12 (2011) 3414.
[22] G.t. Te Velde, F.M. Bickelhaupt, E.J. Baerends, C. Fonseca Guerra, S.J. van Gisbergen, J.G. Snijders, T. Ziegler, J. Comput. Chem. 22 (2001) 931.

SDC EX. 1030 - 7/8

[23] N.E. Gruhn, D.A. da Silva Filho, T.G. Bill, M. Malagoli, V. Coropceanu, A. Kahn, J.-L. Brédas, J. Am. Chem. Soc. 124 (2002) 7918.
[24] S. Kang, T. Kim, Org. Electron. 87 (2020), 105980.
[25] A. Buckingham, J. Del Bene, S. McDowell, Chem. Phys. Lett. 463 (2008) 1.
[26] S. Kang, S.J. Lee, S. Yan, K.C. Nam, J.Y. Lee, J. Incl. Phenom. Macrocycl. Chem. 66 (2010) 67.
[27] F. Weinhold, J.i. Carpenter, The structure of small molecules and ions, Plenum New York, 1988.

SDC EX. 1030 - 8/8